HHS Public Access

Author manuscript

Neuroscience. Author manuscript; available in PMC 2019 February 02.

Published in final edited form as:

Neuroscience. 2017 August 15; 357: 273–284. doi:10.1016/j.neuroscience.2017.06.011.

Distinct neural processes support post-success and post-error slowing in the stop signal task

Yihe Zhang[1,2], **Jaime S. Ide**[2], **Sheng Zhang**[2], **Sien Hu**[2,3], **Nikola S. Valchev**[2], **Xiaoying Tang**[1], and **Chiang-Shan R. Li**[2,4,5,6]

[1]Department of Biomedical engineering, School of Life Sciences, Beijing Institute of technology, Beijing, China

[2]Department of Psychiatry, Yale University School of Medicine, New Haven, CT

[3]Department of Psychology, State University of New York, Oswego, NY

[4]Department of Neuroscience, Yale University School of Medicine, New Haven, CT

[5]Interdepartmental Neuroscience Program, Yale University School of Medicine, New Haven, CT

[6]Beijing Huilongguan Hospital, Beijing, China

Abstract

Executive control requires behavioral adaptation to environmental contingencies. In the stop signal task (SST), participants exhibit slower go trial reaction time (RT) following a stop trial, whether or not they successfully interrupt the motor response. In previous fMRI studies, we demonstrated activation of the right-hemispheric ventrolateral prefrontal cortex, in the area of inferior frontal gyrus, pars opercularis (IFGpo) and anterior insula (AI), during post-error slowing (PES). However, in similar analyses we were not able to identify regional activities during post-success slowing (PSS). Here, we revisited this issue in a larger sample of participants (n=100) each performing the SST for 40 minutes during fMRI. We replicated IFGpo/AI activation to PES ($p \leq 0.05$, FWE corrected). Further, PSS engages decreased activation in a number of cortical regions including the left inferior frontal cortex (IFC; $p \leq 0.05$, FWE corrected). We employed Granger causality mapping to identify areas that provide inputs each to the right IFGpo/AI and left IFC, and computed single trial amplitude (STA) of stop trials of these input regions as well as the STA of post-stop trials of the right IFGpo/AI and left IFC. The STA's of the right inferior precentral sulcus and supplementary motor area (SMA) and right IFGpo/AI were positively correlated and the STA's of the left SMA and left IFC were positively correlated (slope > 0, p's≤ 0.01, one-sample t test), linking regional responses during stop success and error trials to

Address correspondence to: C.-S. Ray Li, Connecticut Mental Health Center S112, 34 Park Street, New Haven, CT 06519-1109, U.S.A., Phone: 203-974-7354, chiang-shan.li@yale.edu OR Xiaoying Tang, 715-3 Teaching Building No.5, Beijing Institute of technology, 5 South Zhongguancun Road, Haidian District, Beijing, 100081, China, Phone: 86-010-68915998, xiaoying@bit.edu.cn.

Author contributions

YZ, JSI, XT, and CSL contributed to study design and writing of the manuscript. SZ and SH, and NV contributed to data collection. YZ and JSI contributed to data analysis. All authors contributed to critical reading and revision of the manuscript and approved the final version submitted for review.

those during PSS and PES. These findings suggest distinct neural mechanisms to support PSS and PES.

Keywords

post-signal slowing; go/no-go; cognitive control; error processing; fMRI

Introduction

The stop signal task (SST) is one of most widely used behavioral task to examine the neural processes of cognitive control. By contrasting various events in the SST, we have described regional responses to motor inhibition, error processing, and post-error behavioral adjustment (Li et al., 2008c; Duann et al., 2009; Winkler et al., 2013; Zhang et al., 2015; Manza et al., 2016a). For instance, the thalamus and supplementary motor area (SMA) respond more strongly to stop error compared to stop or go success trials. After committing an error participants typically delay their motor response in subsequent go trials, a phenomenon termed post-error slowing (PES). Our previous fMRI study demonstrated higher activation of the right-hemispheric ventrolateral prefrontal cortex (VLPFC) during post-error go trials when participants slowed down in reaction time (RT) than during those trials when they did no slow down (Li et al., 2008c). Further, we employed Granger causality mapping (GCM) to query the whole brain for activities that provide inputs to the VLPFC (Ide and Li, 2011b). The results showed that the cerebellum, thalamus, supplementary motor area (SMA) in a cortical pontine cerebellar thalamic circuit respond to stop errors in relation to the RT of subsequent go trials. These findings elucidated the neural correlates of PES and established a directional link between error and post-error responses in the brain.

Participants slowed down in go trial RT not only after stop error but also after stop success trials (Rieger and Gauggel, 1999; Schachar et al., 2004; Mirabella et al., 2006; Li et al., 2008c). In fact, in studies of saccade countermanding in humans and macaque monkeys, the effect of post-success slowing (PSS) appeared to be stronger than PES (Emeric et al., 2007). Whereas PES and PSS can be characterized under a single conceptual framework that examines how trial history influence prospective behavior (Fecteau and Munoz, 2003; Ide et al., 2013; Hu et al., 2015a), the extent of PES and PSS appears to depend on the behavioral paradigms and instructions, raising the possibility that PES and PSS may involve different neural mechanisms. Indeed, in an earlier electrophysiological study, we combined high-density array electroencephalography and a SST to examine event-related potentials of PES and PSS (Chang et al., 2014). The results showed that the amplitude of N2 is greater during PES but not PSS; in contrast, the peak latency of N2 is longer for PSS but not PES. In fMRI studies of the SST, stop success and error engaged different regional responses (Li et al., 2006; Li et al., 2008d; Ide and Li, 2011a) in association with the outcome of a subsequent stop trial (Hendrick et al., 2010). Further, modulation of dorsolateral prefrontal cortical activity contralaterally to motor effector influenced PES but not behavioral adjustment following a conflict in the SST and Wisconsin Card Sorting Task (Mansouri et al., 2016).

On the other hand, with analyses similar to those employed to show VLPFC activation during PES, we were not able to identify regional responses to PSS, despite the fact that participants slowed down in approximately two thirds of both post-success and post-error go trials (Li et al., 2008c). We speculated that, unlike PES which engages error-triggered proactive control, PSS likely involves a multitude of psychological processes, including hesitancy, such that no single mechanism predominates. However, a related possibility is that participants showed greater variability in how these different processes partake in PSS and a larger sample size may help unraveling the neural processes underlying PSS. Here, we revisited this issue in 100 young adults with two specific aims: first, to replicate VLPFC activation during PES; and second, to explore the neural bases of PSS.

Experimental Procedures:

Subjects

One hundred healthy adults (54 females; 31.2 ± 11.0 years of age) participated in this study, including 25 subjects who participated in an earlier study (Ide and Li, 2011b). All participants signed a written, informed consent in accordance with a protocol approved by the Yale Human Investigation Committee. All participants reported no major medical, neurological, or psychiatric illnesses and denied use of illicit substances. None reported problem drinking (with an Alcohol Use Disorder Identification Test score at 0) or smoking. They also tested negative on urine toxicology screens on the day of fMRI.

Behavioral task

Participants performed a stop signal task (SST) (Li et al., 2009; Hu and Li, 2012), Figure 1A). In the SST go and stop trials were randomized in presentation with an inter-trial-interval of 2 s. Each trial began with a fixation, which, after a fore-period varying from 1 s to 5 s (uniform distribution), turned into a circle – the “go” signal – instructing participants to press a button. The circle disappeared at button press or after 1 s if the participant failed to respond. In a stop trial (about one quarter of all trials), the circle was followed by a ‘cross’ – the stop signal – prompting participants to withhold button press. The trial terminated at button press or after 1 s if the participant withheld the response successfully. The stop signal delay (SSD) or time interval between the go and stop signals started at 200 ms and varied from one stop trial to the next following a staircase procedure; SSD increased and decreased by 67 ms each after a successful and failed stop trial (Levitt, 1971). Participants were trained briefly on the task before imaging and instructed to respond quickly when they saw the go signal but keep in mind that a stop signal might come up. They completed four 10-minute sessions of the task with approximately 100 trials in each session during fMRI.

Functional magnetic resonance imaging

Imaging protocol and data pre-processing—T1-weighted spin-echo sagittal anatomical images were acquired for slice localization with a 3-Tesla Siemens Trio scanner (Erlangen, Germany). Anatomical images of the functional slice locations were obtained with spin-echo imaging in an axial plan parallel to the anterior commissure–posterior commissure (AC–PC) line with the following parameters: TR = 300 ms, TE =2.5 ms, bandwidth = 300 Hz/pixel, flip angle = 60°, field of view =220 × 220 mm, matrix = 256 ×

256, 32 slices with slice thickness =4 mm and no gap. A single high-resolution T1-weighted gradient-echo scan was also obtained, with 176 slices parallel to the AC–PC line covering the whole brain: TR = 2530 ms, TE = 3.66 ms, bandwidth = 181 Hz/pixel, flip angle = 7°, field of view = 256 × 256 mm, matrix = 256 × 256, 1 mm^3 isotropic voxels. Blood oxygenation level dependent (BOLD) signals were acquired with a single-shot gradient-echo echo-planar imaging (EPI) sequence in 32 axial slices parallel to the AC–PC line covering the whole brain: TR = 2000 ms, TE = 25 ms, bandwidth = 2004 Hz/pixel, flip angle = 85°, field of view =220 × 220 mm, matrix = 64 × 64, slice thickness =4 mm (no gap). There were 300 images in each session for a total of 4 sessions.

Data were analyzed with Statistical Parametric Mapping (SPM). BOLD images were corrected for realignment and slice timing. A mean functional volume was constructed for each participant for each run from the realigned images. These mean images were then co-registered with the high resolution structural image and segmented for normalization to a Montreal Neurological Institute (MNI) EPI template with affine registration and nonlinear transformation (Friston et al., 1995; Ashburner and Friston, 1999). Finally, images underwent smoothing with an 8 mm (full width at half maximum) Gaussian kernel. Images of the first 5 TRs were discarded.

Generalized linear model (GLM)

Our goal was to isolate the neural processes involved in post-error slowing (PES) and post-success slowing (PSS). As in our previous work (Li et al., 2008c), four trial outcomes were distinguished first: go success (G), go error (F), stop success (SS), and stop error (SE) trial (Figure 1B). G trials were divided into those that followed a G (pG), F (pF), SS (pSS), and SE (pSE) trial, and pSS and pSE trials were further divided into those that increased in RT (pSSi and pSEi, respectively) and those that did not increase in RT (pSSni and pSEni). To determine whether a pSS/pSE trial increased or did not increase in RT, it was compared to the mean RT of all preceding pG trials during each session. The pG trials following the pSS/pSE trial were not considered in that they could not influence the pSS or pSE trial in question. The SS trials that preceded pSSi/pSSni trials were named SSi/SSni and the SE trials that preceded pSEi/pSEni trials were named SEi/SEni, respectively. Across subjects, there were a total of 16.8 ± 4.0 (mean ± SD) “pair” of SSi and pSSi trials, 16.4 ± 4.1 SSni and pSSni trials, 16.2 ± 4.1 SEi and pSEi, and 16.4 ± 4.1 SEni and pSEni trials.

A single GLM was built for each individual subject; go signal onset in each of the trial types was convolved with a canonical hemodynamic response function (HRF) and with the temporal derivative of the canonical HRF (Friston et al., 1995). All 6 realignment parameters were also entered in the GLM. Serial autocorrelation of the time series was corrected using first-degree autoregression (Friston et al., 2000; Della-Maggiore et al., 2002). We constructed two contrast images – pSSi vs. pSSni and pSEi vs. pSEni – to identify regional activations to PSS and PES, respectively, in random effect analysis. All voxel activations are reported in MNI coordinates.

Whole-brain Granger causality analysis (GCA): Granger Causality Mapping (GCM)

We employed GCM (Goebel et al., 2003; Roebroeck et al., 2005), as in our previous work (Ide and Li, 2011b), to identify regions that provide inputs to target regions (see Results). In Granger causality analysis (Granger, 1969), one tests whether a variable x Granger causes y using a bivariate autoregressive model. In short, one computes the autoregressive model of y without variable x (the restricted model) and compares the residual sum of squares RSS_r of variable y with the one from the unrestricted model (autoregressive model of y including x). The residual sum of squares y of is given by: $RSS = \sum_{t=1}^{T} (y(t) - \hat{y}(t))^2 = \sum_{t=1}^{T} \varepsilon(t)^2$, where $\hat{y}$ represents the predicted value of y. The influence from $x \rightarrow y$ can be measured by the fractional F-value (Marquez, 1995):

$$F = \frac{(RSS_r - RSS_{ur})/p}{RSS_{ur}/(T - 2p - 1)} \quad (1)$$

where RSS_{ur} $x \in X$ is the residual sum of squares of variable y in the unrestricted model, p is the model order, and T is the sample size. Variable x causes y, if $F > F_{critical}$ (i.e., the inclusion of variable x significantly decreases the residual error). We employed the Akaike Information Criterion (AIC) to determine the model order with a complexity penalty on the number of parameters to avoid over-fitting (Aiaike, 2008).

Another connectivity measure was proposed by Geweke, in which linear dependence in the time domain from $x \rightarrow y$ (bivariate case) is quantified by (Geweke, 1982; Goebel et al., 2003):

$$F_{x \rightarrow y} = \ln \frac{\left|\mathrm{var}\left(\varepsilon_y^*(t)\right)\right|}{\left|\mathrm{var}\left(\varepsilon_y(t)\right)\right|} \quad (2)$$

where $\varepsilon_y(t)$ is the residual of variable y in the unrestricted model and ε_y^* is the residual of variable y in restricted model, i.e. autoregressive modeling without x variable. Analogously, variable x causes y, if $F_{x \rightarrow y} > F_{x \rightarrow y}(critical)$.

For statistical significance testing, the F-distribution can be used to compute the $F_{critical}$ of Equation (1), assuming independence of residuals, and χ^2 -distribution can be employed to compute the $F_{x \rightarrow y}(critical)$ of Equation (2) (Geweke, 1982; Bressler and Seth, 2011). However, since autoregressive modeling may involve highly interdependent residuals (Deshpande et al., 2009). We used permutation resampling (Hesterberg et al., 2005; Seth, 2010) in statistical test of causality as there are no analytical statistical distributions for the influence measures (Roebroeck et al., 2005). Empirical null distributions of no causality were computed by producing surrogate data (Theiler et al., 1992) as in earlier EEG (Kaminski et al., 2001; Kus et al., 2004) and fMRI work (Deshpande et al., 2009) to derive the critical causality measures. We randomly generated time series with the same mean, variance, autocorrelation function, and spectrum as the original data, to form the surrogate

data (Theiler et al., 1992). In the surrogate data, thus, the causal phase relationships were eliminated with significant connectivity occurring solely by chance.

In GCM the difference of influence measure ($F_{x\to y} - F_{y\to x}$) across the whole brain, i.e., $x \in X$ where X represents the set of brain voxels, was computed with its statistical significance estimated. Equation (2) was used to compute the difference terms, as in (Goebel et al., 2003). It has been suggested that, because the difference term increases specificity (Roebroeck et al., 2005), using the difference term ($F_{x\to y} - F_{y\to x}$), instead of $F_{x\to y}$, is more appropriate for inferring the unilateral connectivity x→y.

PES and PSS each involved activations of the right VLPFC and left inferior frontal cortex (left IFC) at a threshold of voxel p≤0.05, corrected for family-wise error of multiple comparisons (see Results). With GCM we examined which brain regions Granger-cause right VLPFC and left IFC (Goebel et al., 2003; Roebroeck et al., 2005). For each subject, the preprocessed time series were averaged across all voxels within the target region and concatenated across all sessions (each with 295 time points) after linear detrending and normalization (Ding et al., 2000). We used the right VLPFC and left IFC mask each as the target region to compute the voxel-wise Granger causality map for all 100 subjects. That is, we obtained a whole brain map of ($F_{x\to y} - F_{y\to x}$) values for each subject.

In group analysis the median across subjects was used as group statistic and tested against an empirical null distribution constructed from surrogate data (Theiler et al., 1992). For each single voxel in the brain, we tested the significance of voxel - target region connectivity with the following procedures: 1) we computed the median influence difference, $m = \overline{F_{x\to y} - F_{y\to x}}$ across 100 subjects; 2) constructed the empirical distribution of the null "no connectivity" hypothesis, generating 500 samples of surrogate data per subject for averaging; 3) estimated the corresponding $m_{critical}$ from the empirical distribution for a given p-value; and 4) compared m with the critical value and concluded that target region (y) was caused by voxel x if $m > m_{critical}$. The median across subjects is robust against outliers (Sato et al., 2009). The latter study used resampled residuals, but here we employed surrogate data to produce the null distribution (Theiler et al., 1992), as established in earlier work (Kaminski et al., 2001; Kus et al., 2004; Deshpande et al., 2009).

Single Trial Amplitude

We computed and cross-correlated for each individual subject the single trial amplitude (STA) of regions of interest (ROIs), which included the two target regions – right VLPFC and left IFC – and their respective input regions. We obtained the STAs by fitting a design matrix comprising predictors for the onset times of each trial (Eichele et al., 2008). As in the GLM, the onsets were convolved with a canonical HRF and with its temporal derivative. Least squares were employed to estimate the scaling coefficients (β) in the multiple linear regression model with the β estimates taken as the STA. Thus, STA represented a separate analysis independent from the GCM, which examined correlations between the entire time series.

The goal was examine whether the STA of input regions to the right VLPFC and left IFC (as identified from GCM) each during stop error and success trials are correlated with the STA

of right VLPFC and left IFC during post-stop error and post-stop success go trials, respectively. For each participant, we extracted the STA of SE trials for (input regions of right VLPFC) the thalamus, insula, inferior precentral sulcus, precuneus, and supplementary motor area (SMA; see Results); and the STA of SS trials for (input regions of left IFC) the posterior insula and SMA. We also extracted the STA of pSE trials for the right VLPFC and of pSS trials for the left IFC. These two sets of STA's were correlated pairwise with a Pearson regression for each individual subject. We used a one sample test to examine whether the mean of the 100 slopes (one for each participant) was significantly different from zero for each of the 7 sets of correlations − 5 for PES and 2 for PSS. The results were examined at a corrected threshold of p=0.05/7=0.0071.

Results

Behavioral data

Table 1 shows the behavioral results from the stop signal task (SST). The stop success rate is approximately 52% across subjects, indicating the utility in staircasing the SSD. The stop signal reaction time (SSRT) averaged at 203 ms, in the range as reported previously (Yan and Li, 2009; Farr et al., 2012; Hu et al., 2014b; Zhang et al., 2015).

Figure 1C shows pairwise difference in RT between post-go go (pG), post-stop success go (pSS) and post-stop error go (pSE) trials. Compared to pG, both pSS and pSE trials were significantly increased in RT ($t(98)=3.37$, $p\leq0.001$ and $t(98)=4.07$, $p\leq0.0001$, respectively, paired-sample t test) but there was no difference between pSS and pSE trials ($t(98)=0.73$, $p>0.468$). Further, the extent of PES and PSS was correlated across subjects in a linear regression ($r= 0.3823$, $p\leq0.0001$, Figure 1D).

Imaging data – GLM

At $p\leq0.05$, corrected for family-wise error (FWE) of multiple comparisons, right ventrolateral prefrontal cortex, in the area of inferior frontal gyrus, pars opercularis (IFGpo) and anterior insula (AI), showed greater activations during pSEi than pSEni trials. At the same threshold, the left inferior frontal cortex (IFC) showed less activations during pSSi than pSSni trials. When we used voxel $p\leq0.001$, uncorrected in combination with a cluster threshold $p\leq0.05$, FWE corrected, the findings from the contrast pSEi vs. pSEni remained the same. However, a few more areas showed significantly less activations during pSSi than pSSni trials. These brain regions are shown in Figure 2 and summarized in Table 2.

Imaging data – Granger causality mapping (GCM)

We used GCM to explore brain regions with Granger causal inputs each to the right IFGpo/AI and left IFC. Because GCM examines the entire time series rather than addressing the temporal relationship between specific events, we used a liberal threshold to evaluate the results, as in our previous work (Ide and Li, 2011b). The results showed that, at $p\leq0.01$, uncorrected, right middle frontal gyrus, right posterior insula, bilateral thalamus, precuneus and right supplementary motor area (SMA) provide inputs to the right IFGpo/AI (Figure 3A). At the same threshold, right posterior insula and superior temporal gyrus as well as the left SMA provide inputs to the left IFC. These brain regions thus contain potential signals

during stop trials that may relate to responses during post-stop trials. As GCM identified voxels that were causally related for the entire time series, we employed single trial amplitude analyses to confirm the even-related relationship between the input and target regions.

Single trial amplitude (STA)

We next examined whether the activities of input regions identified with GCM and right IFGpo/AI and left IFC – the target regions – are related. As discussed earlier, the analysis of STA was based on GLM and thus distinct from GCM, which examined correlations between the entire time series. Therefore, the findings from STA would provide independent evidence confirming the functional roles of the ROIs identified from GCM. We derived the STAs for each of these input regions as well as the two target regions. Specifically, the STAs of stop errortrials for the thalamus, right posterior insula, right inferior precentral sulcus (IPcS), precuneus (PCu), and right supplementary motor area (SMA) and the STA of right IFGpo/AI of post-error go trials were computed for individual subjects. We performed a linear regression for the STA between each of the five input regions and right IFGpo/AI. Likewise, the STAs of stop success trials for posterior insula/superior temporal gyrus and left SMA and the STA of left IFC for post-success go trials were computed for individual subjects. We performed a linear regression for the STA between each of the two input regions and right IFGpo/AI. For each regression, we tested whether the mean of slope (from 100 linear regressions, each for an individual subject) was significantly different from zero, at a corrected threshold of $p=0.05/7=0.0071$.

Figure 4A and 4B show these regression lines aligned at an intercept of zero for better visualization of the overall pattern of the slopes. At the corrected threshold, the slope of the linear regression between STA of stop error trials for the right IPcS ($t(99)=4.22$, $p\leq0.0001$) and right SMA ($t(99)=3.49$, $p\leq0.001$) and the STA of post-error go trials for right IFGpo/AI was significantly different from zero; and the slope of the linear regression between STA of stop success trials for the left SMA was significantly correlated with the STA of post-success go trials for left IFC ($t(99)=10.21$, $p<0.0001$).

Discussion

We showed that right ventrolateral prefrontal cortex, in the area of inferior frontal gyrus, pars operculum and anterior insula (IFGpo/AI) increased activation to post-error slowing (PES), whereas a set of regions, including the left inferior frontal cortex (IFC), decreased activation to post-success slowing (PSS). Granger causality mapping (GCM) identified regions that provide inputs each to the right IFGpo/AI and left IFC. Further, analysis of single trial amplitude (STA) showed that activities of the right-hemispheric thalamus, inferior precentral sulcus, and supplementary motor area (SMA) during stop error trials were positively correlated with activities of the right IFGpo/AI during post-error go trials; and activities of the left-hemispheric SMA during stop success trials were positively correlated with activities of the left IFC during post-success go trials. In addition to replicating our earlier findings (Li et al., 2008c; Ide and Li, 2011b), these results revealed the neural bases of post-success slowing.

Hemispheric asymmetry in behavioral control

PES involved greater activation of the right IFGpo/AI while PSS involved less activation of the left IFC, suggesting greater control over delayed responses following errors and over speeded responses following successes and hemispheric functional asymmetry of these prefrontal cortical structures. Hemispheric specialization appears to be a common feature for heteromodal association cortex (Zilles et al., 1996). Although rarely a focus of imaging studies, hemispheric asymmetry in the neural processes of cognitive control has been reported in the literature. For instance, transcranial direct current stimulation showed opposite effects on the right versus left prefrontal cortex in affective decision making (Pripfl et al., 2013). In a resting-state electroencephalographic study, individuals with stronger left/right-lateralized intrinsic activity in the middle frontal gyrus were respectively more capable of phasic/sustained cognitive control during task switching (Ambrosini and Vallesi, 2016). The findings suggest prefrontal hemispheric asymmetry to support individual differences in responses to changing task demands. A number of functional connectivity studies documented hemispheric differences in network organization (Liu et al., 2009; Tomasi and Volkow, 2012; Gotts et al., 2013). For instance, the frontoparietal control network is preferentially coupled to the left-hemispheric default network regions but to right-hemispheric attention networks (Wang et al., 2014). Right-hemispheric functional connectivity between the presupplementary motor area and caudate nucleus – structures of critical importance to inhibitory control (Li et al., 2006; Li et al., 2008b; Chao et al., 2009; Duann et al., 2009) – is stronger than left-hemispheric connectivity (Zhang et al., 2012). In accord with the current findings, response speeding involves activation largely of the left-hemispheric cortical and subcortical structures in the stop signal task (Li et al., 2009). Together, these findings support hemispheric functional differentiation for cognitive control, with right- and left- hemispheric activity each dominating control of “avoidance” and “approach” behavior.

Frontal functional asymmetry has been related to avoidance and approach behavior (Harmon-Jones et al., 2010; Rutherford and Lindell, 2011). Greater left frontal activity has been associated with sensation seeking (Santesso et al., 2008), positive urgency (Gable et al., 2015), and impulsivity (Neal and Gable, 2016), whereas greater right frontal activity has been associated with risk aversion (Gianotti et al., 2009). The relationship between hemispheric functional asymmetry and behavioral approach/avoidance appears to extend beyond the frontal cortical system. For instance, in fMRI, novelty seeking is correlated with the extent of left lateralization of anterior insula connectivity to the pallidum and putamen in men (Kann et al., 2016). Participants with increased reward response in the left and right nucleus accumbens displayed better approach and avoidance learning, respectively (Aberg et al., 2015). The latter findings are consistent with studies of dopamine D2 receptor binding potential as a predictor of reward and punishment sensitivity (Tomer et al., 2014) and of asymmetric dopaminergic neuronal loss and associated behavioral changes in individuals with Parkinson’s disease (PD) (Maril et al., 2013; Porat et al., 2014). When off medications, PD patients with left-hemispheric dopaminergic deficits minimized losses better than increasing gains, while those with predominantly right-hemispheric deficits demonstrated a trend toward the opposite. It would be of great interest for future studies to examine how

frontal control system interacts with subcortical reward circuits in determining approach and avoidance.

Neural bases of post-error slowing and post-success speeding

Post-error slowing (PES) engages robust activation in the right-hemispheric inferior frontal gyrus, pars opercularis (IFGpo) and anterior insula (AI). The rIFC and rAI co-activate for response inhibition in the stop signal task, as shown in a recent meta-analysis (Cai et al., 2014). However, in distinguishing the two structures, authors noted that the rAI showed stronger task-evoked and intrinsic functional connectivity with the anterior cingulate cortex (ACC), whereas the rIFC had stronger connectivity with dorsomedial prefrontal and lateral fronto-parietal cortices. The rAI showed greater activation than the rIFC during stop error but not during stop success trials, and multivoxel response profiles in the rAI, but not the rIFC, accurately differentiated between stop success and error. A multivariate dynamic systems analysis demonstrated greater causal interaction from rAI to dorsal ACC on trials with high than with low demand for control and in significant correlation with individual differences in cognitive control abilities (Cai et al., 2016). Further, activation of the rIFC, but not rAI, predicted individual capacity in inhibitory control. These findings dissociate the roles of the two regions in inhibitory control, with rAI dominating in saliency detection and rIFC in the implementation of inhibitory control (Chikazoe et al., 2009).

In contrast, post-success slowing involves less activation in the left inferior frontal cortex (IFC). That is, the left IFC responded to post-success go trials where participants speeded up in RT than trials where they slowed down. This finding of left IFC response to post-success speeding is intriguing in that it seemingly contrasts with previous studies that support a role of the left IFC in response inhibition (Swick and Chatham, 2014; Schmuser et al., 2016). On the other hand, by distinguishing contextual effects in an item recency judgment task, Jimura and colleagues showed that the left IFC is involved in inhibition of proactive interference rather than inhibition of inappropriate responses per se (Jimura et al., 2009). Thus, the left IFC may increase activation to overcome the interference generated from conflict or conflict anticipation, as required when participantswere to speed up following a stop success trial. Further, activation of the left IFC has been implicated in the expression of expertise in mathematics (Jeon and Friederici, 2016), visuomotor control (Papadelis et al., 2016), and, perhaps the best known, in verbal skills (Becker et al., 2016; Canini et al., 2016; Leminen et al., 2016; Vogelsang et al., 2016). It is possible that post-success speeding reflects experience-based strategic decision and engages the left IFC. The decision to speed up is likely to be effortful, as it contrasts with learning based on trial history that indicates a need of increased control of RT following a stop signal (Ide et al., 2013; Hu et al., 2015a). Indeed, in a previous fMRI study, participants exerted self control by performing thought suppression (or not, as a control) before being engaged in a Stroop task (Luethi et al., 2016). Compared to control, participants performed worse on the Stroop task along with decreased left IFC activation, suggesting that left IFC activity may reflect effort and arousal (Urgesi et al., 2016) that is required across different behavioral challenges. Also in support of a role of the left IFC in sustaining attention and effort were imaging studies reporting a detrimental effect of its signal variability on cognitive stability, as shown in increased response time costs during distractor inhibition (Armbruster-Genc et al., 2016) and increased switch cost in

a switching task in association with less functional connectivity of the left IFC (Yin et al., 2015). More broadly, structural connectivity between the left IFC and subcortical structures was implicated in integrating favorable (in terms of motivational valence) information into beliefs but less so with unfavorable information (Moutsiana et al., 2015). One is tempted to speculate that stop success trial conveys favorable information and, with left IFC activation, participants were encouraged to speed up as they believed they were "doing things right." Another study demonstrated greater activation of the left IFC when participants used logic to inhibit biased thoughts in problem solving (Luo et al., 2014). This is perhaps analogous to the process to overcome the response bias (to delay a go response) following a stop success in the SST.

Notably, the left IFC can be parcellated into functional subclusters, with a cluster at the posterior end of the inferior frontal sulcus (IFS) matching previous descriptions of the inferior frontal junction (IFJ) in location, a caudal cluster involved in motor control, a ventral cluster for linguistic processing, and 3 more rostral clusters involved in other aspects of cognitive control (Muhle-Karbe et al., 2016). In the current findings, the peak location of the left IFC (x=−45, y=26, z=19) appeared to correspond best to the IFG (x=−51, y=25, z=21) and aIFS (x=−36, y=25, z=19) clusters. Analysis for whole brain co-activation patterns showed that these clusters shared connectivities to the frontoparietal control network but also exhibited distinct connectivities, with the IFG connected specifically to large parts of the left IFG, as well as with the left middle and inferior temporal gyri and the aIFS connected to its right homotope and the rostral anterior cingulate cortex. Functionally, the IFG cluster showed the strongest association with language and semantic memory and the aIFS cluster was most strongly associated with functions related to interference resolution and attention shifts. While these findings may not offer specific insights why the left IFC responds to post-success speeding, they suggest the complexity in left IFC functions and of the psychological processes involved in the decision not to slow down following a stop success trial in the SST.

Supplementary motor area (SMA) activity as a potential "trigger" for PES and PSS

As in our earlier study, we observed that activity of the SMA preceded and Granger caused activations of the rIFGpo/AI during PES and left IFC during PSS. Interconnected with primary motor and premotor structures, the SMA is involved in motor control showing similar activations during SE vs. G trials and less activations during SS vs. G trials (Li et al., 2008a). Greater activation of the SMA is associated with prolonged response time (Hu et al., 2014a; Hu et al., 2015a). Activity of the right inferior precentral sulcus (IPcS), in the primary motor cortical "hand" area, during errors also preceded and Granger caused activity of the rIFGpo/AI during PES. As bilateral primary motor cortices are reciprocally inhibited via transcallosal connections (Irlbacher et al., 2007; Palmer et al., 2012), greater activity of the right IPcS (ipsilateral to motor response) would also relateto prolonged response time. These findings together suggest that altered activity of the motor structures during stop trials precedes post-stop behavioral adjustment, consistent with an earlier transcranial magnetic stimulation study showing a decrease in the motor cortical excitability after an erroneous response in the flankers task (Amengual et al., 2013). This modulation of corticospinal activity may serve to prevent further premature and erroneous responses; "choked" motor

processes during a stop trial may precede post-stop slowing. More studies are needed to further examine to what extent this transpires via interactions between motor cortical structures, within cortical subcortical circuits, and/or at the neuromuscular machinery.

Implications for computational modeling of SST performance

To characterize the influence of post-signal adjustment in RT, we have previously employed a Bayesian belief model to quantify the trial-by-trial likelihood of a stop signal – P(Stop) – and described a linear positive relationship between the P(Stop) and RT of go trials, which we termed "sequential effect" (Ide et al., 2013; Hu et al., 2015a). The model showed that participants changed their estimate of P(Stop) upon each occurrence of a stop signal and when P(Stop) is high, they were more likely to slow down in RT and less likely to commit an error (Hu et al., 2015b; Ide et al., 2015; Manza et al., 2016b). Further, the magnitude of the sequential effect is positively correlated with PES and PSS. On the other hand, the current findings showed that PES and PSS involve distinct neural processes, suggesting that the stop error and stop success may need to be modeled as different events to fully capture SST performance. Likewise, rather than simply anticipating conflict, participants may specifically anticipate a stop success or error and these cognitive complexities require further investigation in computational modeling of cognitive control.

Limitations of the study

A critical limitation of the study is the uncorrected threshold we used to explore input activities to support PES and PSS. While the use of an uncorrected threshold does not conform to current standard in reporting imaging findings, we wish to emphasize the standard speaks largely to reporting from generalized linear models. Nonetheless, the current GCM results should best be considered as preliminary and replicated in future work. Another limitation concerns the lack of cerebellar and pontine activity as inputs to rIFC/AI during PES, in contrast to our previous work (Ide and Li, 2011a). This non-replication suggests that cerebellar and pontine activities may not serve a consistent role in the neural circuits of PES. We should also acknowledge that the fundamental psychological processes underlying PSS remains unclear. Although we described the literature of left IFC activation and possible psychological analogues of this process, this discussion remains speculative. What seems to be clear is that neither PSS or PES represents a reflexive response to the stop signal (Bissett and Logan, 2012). Rather, post-signal slowing involves strategic adjustment of response that may require learning, anticipation and potentially a host of other processes that remain to be understood (Li et al., 2008d; Hu et al., 2016a). Finally, although the STA of input and targets regions were positively correlated for the majority of the participants, there was substantial inter-subject variation. For instance, individuals who showed a positive vs. negative slope in STA correlations did not appear to exhibit differences in SST performance, including the extent of PSS and PES (data not shown). Thus, while the current findings demonstrate the neural bases of post-signal behavioral adjustment within subjects, studies are needed to address individual variation, as with what we have shown earlier for stop signal reaction time and control of impulsive response (Hu et al., 2016b).

Acknowledgements

This study was supported by NSF grant BCS1309260 and NIH grants AA021449 and DA023248, as well as research funding provided by Beijing Institute of Technology. The funding agencies had no further role in study design; in the collection, analysis and interpretation of data; in the writing of the report; or in the decision to submit the paper for publication.

Abbreviations

SST	stop signal task
RT	reaction time
IFGpo	inferior frontal gyrus, pars opercularis
AI	anterior insula
L	left
R	right
IFC	inferior frontal cortex
S	sulcus
MFG	middle frontal gyrus
OFG	orbitofrontal gyrus
G	gyrus
SMA	supplementary motor area
VLPFC	ventrolateral prefrontal cortex
IPcS	right inferior precentral sulcus
PCu	precuneus
IFS	inferior frontal sulcus
IFJ	inferior frontal junction
PES	post-error slowing
PSS	post-success slowing
GCA	Granger causality analysis
GCM	Granger causality mapping
AC–PC	anterior commissure–posterior commissure
BOLD	blood oxygenation level dependent
EPI	echo-planar imaging

MNI	Montreal Neurological Institute
GLM	Generalized linear model
G	go success
F	go error
SS	stop success
SE	stop error
pG	post-go
pSS	post-stop success
pSE	post-stop error
HRF	hemodynamic response function
STA	single trial amplitude
ROI	regions of interest
GS (%)	percentage of successful go trials
SS (%)	percentage of successful stop trials
Mean/Median GoRT	mean/median of go trial reaction time
SERT	stop error reaction time
SSRT	stop signal reaction time
FWE	family-wise error
PD	Parkinson's disease

References

Aberg KC, Doell KC, Schwartz S (2015) Hemispheric Asymmetries in Striatal Reward Responses Relate to Approach-Avoidance Learning and Encoding of Positive-Negative Prediction Errors in Dopaminergic Midbrain Regions. J Neurosci 35:14491–14500. [PubMed: 26511241]

Aiaike H (2008) A new look at the statistical model indentification' IEEE Transactions on Automatic Control. Automatic Control IEEE Transactions on 19:716–723.

Ambrosini E, Vallesi A (2016) Asymmetry in prefrontal resting-state EEG spectral power underlies individual differences in phasic and sustained cognitive control. Neuroimage 124:843–857. [PubMed: 26416650]

Amengual JL, Marco-Pallares J, Richter L, Oung S, Schweikard A, Mohammadi B, Rodriguez-Fornells A, Munte TF (2013) Tracking post-error adaptation in the motor system by transcranial magnetic stimulation. Neuroscience 250:342–351. [PubMed: 23876325]

Armbruster-Genc DJ, Ueltzhoffer K, Fiebach CJ (2016) Brain Signal Variability Differentially Affects Cognitive Flexibility and Cognitive Stability. J Neurosci 36:3978–3987. [PubMed: 27053205]

Ashburner J, Friston KJ (1999) Nonlinear spatial normalization using basis functions. Hum Brain Mapp 7:254–266. [PubMed: 10408769]

Becker M, Schubert T, Strobach T, Gallinat J, Kuhn S (2016) Simultaneous interpreters vs. professional multilingual controls: Group differences in cognitive control as well as brain structure and function. Neuroimage 134:250–260. [PubMed: 27085505]

Bissett PG, Logan GD (2012) Post-stop-signal slowing: strategies dominate reflexes and implicit learning. J Exp Psychol Hum Percept Perform 38:746–757. [PubMed: 21895385]

Bressler SL, Seth AK (2011) Wiener-Granger causality: a well established methodology. Neuroimage 58:323–329. [PubMed: 20202481]

Cai W, Ryali S, Chen T, Li CS, Menon V (2014) Dissociable roles of right inferior frontal cortex and anterior insula in inhibitory control: evidence from intrinsic and task-related functional parcellation, connectivity, and response profile analyses across multiple datasets. J Neurosci 34:14652–14667. [PubMed: 25355218]

Cai W, Chen T, Ryali S, Kochalka J, Li CS, Menon V (2016) Causal Interactions Within a Frontal-Cingulate-Parietal Network During Cognitive Control: Convergent Evidence from a Multisite-Multitask Investigation. Cereb Cortex 26:2140–2153. [PubMed: 25778346]

Canini M, Della Rosa PA, Catricala E, Strijkers K, Branzi FM, Costa A, Abutalebi J (2016) Semantic interference and its control: A functional neuroimaging and connectivity study. Hum Brain Mapp 37:4179–4196. [PubMed: 27355179]

Chang A, Chen CC, Li HH, Li CS (2014) Event-related potentials for post-error and post-conflict slowing. PLoS One 9:e99909. [PubMed: 24932780]

Chao HH, Luo X, Chang JL, Li CS (2009) Activation of the pre-supplementary motor area but not inferior prefrontal cortex in association with short stop signal reaction time--an intra-subject analysis. BMC Neurosci 10:75. [PubMed: 19602259]

Chikazoe J, Jimura K, Asari T, Yamashita K, Morimoto H, Hirose S, Miyashita Y, Konishi S (2009) Functional dissociation in right inferior frontal cortex during performance of go/no-go task. Cereb Cortex 19:146–152. [PubMed: 18445602]

Della-Maggiore V, Chau W, Peres-Neto PR, McIntosh AR (2002) An empirical comparison of SPM preprocessing parameters to the analysis of fMRI data. Neuroimage 17:19–28. [PubMed: 12482065]

Deshpande G, LaConte S, James GA, Peltier S, Hu X (2009) Multivariate Granger causality analysis of fMRI data. Hum Brain Mapp 30:1361–1373. [PubMed: 18537116]

Ding M, Bressler SL, Yang W, Liang H (2000) Short-window spectral analysis of cortical event-related potentials by adaptive multivariate autoregressive modeling: data preprocessing, model validation, and variability assessment. Biol Cybern 83:35–45. [PubMed: 10933236]

Duann JR, Ide JS, Luo X, Li CS (2009) Functional connectivity delineates distinct roles of the inferior frontal cortex and presupplementary motor area in stop signal inhibition. J Neurosci 29:10171–10179. [PubMed: 19675251]

Eichele T, Debener S, Calhoun VD, Specht K, Engel AK, Hugdahl K, von Cramon DY, Ullsperger M (2008) Prediction of human errors by maladaptive changes in event-related brain networks. Proc Natl Acad Sci U S A 105:6173–6178. [PubMed: 18427123]

Emeric EE, Brown JW, Boucher L, Carpenter RH, Hanes DP, Harris R, Logan GD, Mashru RN, Pare M, Pouget P, Stuphorn V, Taylor TL, Schall JD (2007) Influence of history on saccade countermanding performance in humans and macaque monkeys. Vision Res 47:35–49. [PubMed: 17081584]

Farr OM, Hu S, Zhang S, Li CS (2012) Decreased saliency processing as a neural measure of Barratt impulsivity in healthy adults. Neuroimage 63:1070–1077. [PubMed: 22885245]

Fecteau JH, Munoz DP (2003) Exploring the consequences of the previous trial. Nat Rev Neurosci 4:435–443. [PubMed: 12778116]

Friston KJ, Mechelli A, Turner R, Price CJ (2000) Nonlinear responses in fMRI: the Balloon model, Volterra kernels, and other hemodynamics. Neuroimage 12:466–477. [PubMed: 10988040]

Friston KJ, Holmes AP, Poline JB, Grasby PJ, Williams SC, Frackowiak RS, Turner R (1995) Analysis of fMRI time-series revisited. Neuroimage 2:45–53. [PubMed: 9343589]

Gable PA, Mechin NC, Hicks JA, Adams DL (2015) Supervisory control system and frontal asymmetry: neurophysiological traits of emotion-based impulsivity. Soc Cogn Affect Neurosci 10:1310–1315. [PubMed: 25678550]

Geweke J (1982) Measurement of linear dependence and feedback between multiple time series. Journal of the American statistical association 77:304–313.

Gianotti LR, Knoch D, Faber PL, Lehmann D, Pascual-Marqui RD, Diezi C, Schoch C, Eisenegger C, Fehr E (2009) Tonic activity level in the right prefrontal cortex predicts individuals' risk taking. Psychol Sci 20:33–38. [PubMed: 19152538]

Goebel R, Roebroeck A, Kim DS, Formisano E (2003) Investigating directed cortical interactions in time-resolved fMRI data using vector autoregressive modeling and Granger causality mapping. Magn Reson Imaging 21:1251–1261. [PubMed: 14725933]

Gotts SJ, Jo HJ, Wallace GL, Saad ZS, Cox RW, Martin A (2013) Two distinct forms of functional lateralization in the human brain. Proc Natl Acad Sci U S A 110:E3435–3444. [PubMed: 23959883]

Granger CWJ (1969) Investigating causal relations by econometric models and cross-spectral methods. Econometrica 37:424–438.

Harmon-Jones E, Gable PA, Peterson CK (2010) The role of asymmetric frontal cortical activity in emotion-related phenomena: a review and update. Biol Psychol 84:451–462. [PubMed: 19733618]

Hendrick OM, Ide JS, Luo X, Li CS (2010) Dissociable processes of cognitive control during error and non-error conflicts: a study of the stop signal task. PLoS One 5:e13155. [PubMed: 20949134]

Hesterberg T, Monaghan S, Moore DS, Clipson A, Epstein R, Freeman WH, York CN (2005) Bootstrap Methods and Permutation Tests. The Practice of Business Statistics.

Hu J, Hu S, Maisano JR, Chao HH, Zhang S, Li CR (2016a) Novelty Seeking, Harm Avoidance, and Cerebral Responses to Conflict Anticipation: An Exploratory Study. Front Hum Neurosci 10:546. [PubMed: 27857686]

Hu S, Li CS (2012) Neural processes of preparatory control for stop signal inhibition. Hum Brain Mapp 33:2785–2796. [PubMed: 21976392]

Hu S, Tseng YC, Winkler AD, Li CS (2014a) Neural bases of individual variation in decision time. Hum Brain Mapp 35:2531–2542. [PubMed: 24027122]

Hu S, Ide JS, Zhang S, Li CS (2015a) Anticipating conflict: Neural correlates of a Bayesian belief and its motor consequence. Neuroimage 119:286–295. [PubMed: 26095091]

Hu S, Ide JS, Zhang S, Li CR (2016b) The Right Superior Frontal Gyrus and Individual Variation in Proactive Control of Impulsive Response. J Neurosci 36:12688–12696. [PubMed: 27974616]

Hu S, Chao HH, Zhang S, Ide JS, Li CS (2014b) Changes in cerebral morphometry and amplitude of low-frequency fluctuations of BOLD signals during healthy aging: correlation with inhibitory control. Brain Struct Funct 219:983–994. [PubMed: 23553547]

Hu S, Ide JS, Zhang S, Sinha R, Li CS (2015b) Conflict anticipation in alcohol dependence - A model-based fMRI study of stop signal task. Neuroimage Clin 8:39–50. [PubMed: 26106526]

Ide JS, Li CS (2011a) Error-related functional connectivity of the habenula in humans. Front Hum Neurosci 5:25. [PubMed: 21441989]

Ide JS, Li CS (2011b) A cerebellar thalamic cortical circuit for error-related cognitive control. Neuroimage 54:455–464. [PubMed: 20656038]

Ide JS, Shenoy P, Yu AJ, Li CS (2013) Bayesian prediction and evaluation in the anterior cingulate cortex. J Neurosci 33:2039–2047. [PubMed: 23365241]

Ide JS, Hu S, Zhang S, Yu AJ, Li CS (2015) Impaired Bayesian learning for cognitive control in cocaine dependence. Drug Alcohol Depend 151:220–227. [PubMed: 25869543]

Irlbacher K, Brocke J, Mechow JV, Brandt SA (2007) Effects of GABA(A) and GABA(B) agonists on interhemispheric inhibition in man. Clin Neurophysiol 118:308–316. [PubMed: 17174150]

Jeon HA, Friederici AD (2016) What Does "Being an Expert" Mean to the Brain? Functional Specificity and Connectivity in Expertise. Cereb Cortex.

Jimura K, Yamashita K, Chikazoe J, Hirose S, Miyashita Y, Konishi S (2009) A critical component that activates the left inferior prefrontal cortex during interference resolution. Eur J Neurosci 29:1915–1920. [PubMed: 19473243]

Kaminski M, Ding M, Truccolo WA, Bressler SL (2001) Evaluating causal relations in neural systems: granger causality, directed transfer function and statistical assessment of significance. Biol Cybern 85:145–157. [PubMed: 11508777]

Kann S, Zhang S, Manza P, Leung HC, Li CR (2016) Hemispheric Lateralization of Resting-State Functional Connectivity of the Anterior Insula: Association with Age, Gender, and a Novelty-Seeking Trait. Brain Connect 6:724–734. [PubMed: 27604154]

Kus R, Kaminski M, Blinowska KJ (2004) Determination of EEG activity propagation: pair-wise versus multichannel estimate. IEEE Trans Biomed Eng 51:1501–1510. [PubMed: 15376498]

Leminen A, Kimppa L, Leminen MM, Lehtonen M, Makela JP, Shtyrov Y (2016) Acquisition and consolidation of novel morphology in human neocortex: A neuromagnetic study. Cortex 83:1–16. [PubMed: 27458780]

Levitt H (1971) Transformed up-down methods in psychoacoustics. J Acoust Soc Am 49:Suppl 2:467+.

Li CS, Yan P, Chao H-A, Sinha R, Paliwal P, Constable RT, Zhang S, Lee T-W (2008a) Error-specific medial cortical and subcortical activity during the stop signal task: a functional magnetic resonance imaging study. Neuroscience 155:1142–1151. [PubMed: 18674592]

Li CS, Chao HH, Lee TW (2009) Neural correlates of speeded as compared with delayed responses in a stop signal task: an indirect analog of risk taking and association with an anxiety trait. Cereb Cortex 19:839–848. [PubMed: 18678764]

Li CS, Huang C, Constable RT, Sinha R (2006) Imaging response inhibition in a stop-signal task: neural correlates independent of signal monitoring and post-response processing. J Neurosci 26:186–192. [PubMed: 16399686]

Li CS, Yan P, Sinha R, Lee TW (2008b) Subcortical processes of motor response inhibition during a stop signal task. Neuroimage 41:1352–1363. [PubMed: 18485743]

Li CS, Huang C, Yan P, Paliwal P, Constable RT, Sinha R (2008c) Neural correlates of post-error slowing during a stop signal task: a functional magnetic resonance imaging study. J Cogn Neurosci 20:1021–1029. [PubMed: 18211230]

Li CS, Yan P, Chao HH, Sinha R, Paliwal P, Constable RT, Zhang S, Lee TW (2008d) Error-specific medial cortical and subcortical activity during the stop signal task: a functional magnetic resonance imaging study. Neuroscience 155:1142–1151. [PubMed: 18674592]

Liu H, Stufflebeam SM, Sepulcre J, Hedden T, Buckner RL (2009) Evidence from intrinsic activity that asymmetry of the human brain is controlled by multiple factors. Proc Natl Acad Sci U S A 106:20499–20503. [PubMed: 19918055]

Luethi MS, Friese M, Binder J, Boesiger P, Luechinger R, Rasch B (2016) Motivational incentives lead to a strong increase in lateral prefrontal activity after self-control exertion. Soc Cogn Affect Neurosci 11:1618–1626. [PubMed: 27217108]

Luo J, Tang X, Zhang E, Stupple EJ (2014) The neural correlates of belief-bias inhibition: the impact of logic training. Biol Psychol 103:276–282. [PubMed: 25263609]

Mansouri FA, Fehring DJ, Feizpour A, Gaillard A, Rosa MG, Rajan R, Jaberzadeh S (2016) Direct current stimulation of prefrontal cortex modulates error-induced behavioral adjustments. Eur J Neurosci 44:1856–1869. [PubMed: 27207192]

Manza P, Hu S, Chao HH, Zhang S, Leung HC, Li CS (2016a) A dual but asymmetric role of the dorsal anterior cingulate cortex in response inhibition and switching from a non-salient to salient action. Neuroimage 134:466–474. [PubMed: 27126003]

Manza P, Hu S, Ide JS, Farr OM, Zhang S, Leung HC, Li CS (2016b) The effects of methylphenidate on cerebral responses to conflict anticipation and unsigned prediction error in a stop-signal task. J Psychopharmacol 30:283–293. [PubMed: 26755547]

Maril S, Hassin-Baer S, Cohen OS, Tomer R (2013) Effects of asymmetric dopamine depletion on sensitivity to rewarding and aversive stimuli in Parkinson's disease. Neuropsychologia 51:818–824. [PubMed: 23422331]

Marquez J (1995) Time series analysis : James D. Hamilton, 1994, (Princeton University Press, Princeton, NJ), 799 pp., US $55.00, ISBN 0-691-04289-6. International Journal of Forecasting 11:494–495.

Mirabella G, Pani P, Pare M, Ferraina S (2006) Inhibitory control of reaching movements in humans. Exp Brain Res 174:240–255. [PubMed: 16636792]

Moutsiana C, Charpentier CJ, Garrett N, Cohen MX, Sharot T (2015) Human Frontal-Subcortical Circuit and Asymmetric Belief Updating. J Neurosci 35:14077–14085. [PubMed: 26490851]

Muhle-Karbe PS, Derrfuss J, Lynn MT, Neubert FX, Fox PT, Brass M, Eickhoff SB (2016) Co-Activation-Based Parcellation of the Lateral Prefrontal Cortex Delineates the Inferior Frontal Junction Area. Cereb Cortex 26:2225–2241. [PubMed: 25899707]

Neal LB, Gable PA (2016) Neurophysiological markers of multiple facets of impulsivity. Biol Psychol 115:64–68. [PubMed: 26808340]

Palmer LM, Schulz JM, Murphy SC, Ledergerber D, Murayama M, Larkum ME (2012) The cellular basis of GABA(B)-mediated interhemispheric inhibition. Science 335:989–993. [PubMed: 22363012]

Papadelis C, Arfeller C, Erla S, Nollo G, Cattaneo L, Braun C (2016) Inferior frontal gyrus links visual and motor cortices during a visuomotor precision grip force task. Brain Res 1650:252–266. [PubMed: 27641995]

Porat O, Hassin-Baer S, Cohen OS, Markus A, Tomer R (2014) Asymmetric dopamine loss differentially affects effort to maximize gain or minimize loss. Cortex 51:82–91. [PubMed: 24267688]

Pripfl J, Neumann R, Kohler U, Lamm C (2013) Effects of transcranial direct current stimulation on risky decision making are mediated by 'hot' and 'cold' decisions, personality, and hemisphere. Eur J Neurosci 38:3778–3785. [PubMed: 24124667]

Rieger M, Gauggel S (1999) Inhibitory after-effects in the stop signal paradigm. British Journal of Psychology 90:509–518.

Roebroeck A, Formisano E, Goebel R (2005) Mapping directed influence over the brain using Granger causality and fMRI. Neuroimage 25:230–242. [PubMed: 15734358]

Rutherford HJV, Lindell AK (2011) Thriving and Surviving: Approach and Avoidance Motivation and Lateralization. Emotion Review 3:333–343.

Santesso DL, Segalowitz SJ, Ashbaugh AR, Antony MM, McCabe RE, Schmidt LA (2008) Frontal EEG asymmetry and sensation seeking in young adults. Biol Psychol 78:164–172. [PubMed: 18367308]

Sato JR, Takahashi DY, Arcuri SM, Sameshima K, Morettin PA, Baccala LA (2009) Frequency domain connectivity identification: an application of partial directed coherence in fMRI. Hum Brain Mapp 30:452–461. [PubMed: 18064582]

Schachar RJ, Chen S, Logan GD, Ornstein TJ, Crosbie J, Ickowicz A, Pakulak A (2004) Evidence for an error monitoring deficit in attention deficit hyperactivity disorder. J Abnorm Child Psychol 32:285–293. [PubMed: 15228177]

Schmuser L, Sebastian A, Mobascher A, Lieb K, Feige B, Tuscher O (2016) Data-driven analysis of simultaneous EEG/fMRI reveals neurophysiological phenotypes of impulse control. Hum Brain Mapp 37:3114–3136. [PubMed: 27133468]

Seth AK (2010) A MATLAB toolbox for Granger causal connectivity analysis. J Neurosci Methods 186:262–273. [PubMed: 19961876]

Swick D, Chatham CH (2014) Ten years of inhibition revisited. Front Hum Neurosci 8:329. [PubMed: 24904369]

Theiler J, Eubank S, Longtin A, Galdrikian B, Farmer JD (1992) Testing for nonlinearity in time series: the method of surrogate data In: Conference proceedings on Interpretation of time series from nonlinear mechanical systems, pp 77–94.

Tomasi D, Volkow ND (2012) Laterality patterns of brain functional connectivity: gender effects. Cereb Cortex 22:1455–1462. [PubMed: 21878483]

Tomer R, Slagter HA, Christian BT, Fox AS, King CR, Murali D, Gluck MA, Davidson RJ (2014) Love to win or hate to Lose? Asymmetry of dopamine D2 receptor binding predicts sensitivity to reward versus punishment. J Cogn Neurosci 26:1039–1048. [PubMed: 24345165]

Urgesi C, Mattiassi AD, Buiatti T, Marini A (2016) Tell it to a child! A brain stimulation study of the role of left inferior frontal gyrus in emotion regulation during storytelling. Neuroimage 136:26–36. [PubMed: 27188219]

Vogelsang DA, Bonnici HM, Bergstrom ZM, Ranganath C, Simons JS (2016) Goal-directed mechanisms that constrain retrieval predict subsequent memory for new "foil" information. Neuropsychologia 89:356–363. [PubMed: 27431039]

Wang D, Buckner RL, Liu H (2014) Functional specialization in the human brain estimated by intrinsic hemispheric interaction. J Neurosci 34:12341–12352. [PubMed: 25209275]

Winkler AD, Hu S, Li CS (2013) The influence of risky and conservative mental sets on cerebral activations of cognitive control. Int J Psychophysiol 87:254–261. [PubMed: 22922525]

Yan P, Li CS (2009) Decreased amygdala activation during risk taking in non-dependent habitual alcohol users: A preliminary fMRI study of the stop signal task. Am J Drug Alcohol Abuse 35:284–289. [PubMed: 19579091]

Yin S, Wang T, Pan W, Liu Y, Chen A (2015) Task-switching Cost and Intrinsic Functional Connectivity in the Human Brain: Toward Understanding Individual Differences in Cognitive Flexibility. PLoS One 10:e0145826. [PubMed: 26716447]

Zhang S, Ide JS, Li CS (2012) Resting-state functional connectivity of the medial superior frontal cortex. Cereb Cortex 22:99–111. [PubMed: 21572088]

Zhang S, Tsai SJ, Hu S, Xu J, Chao HH, Calhoun VD, Li CS (2015) Independent component analysis of functional networks for response inhibition: Inter-subject variation in stop signal reaction time. Hum Brain Mapp 36:3289–3302. [PubMed: 26089095]

Zilles K, Dabringhaus A, Geyer S, Amunts K, Qu M, Schleicher A, Gilissen E, Schlaug G, Steinmetz H (1996) Structural asymmetries in the human forebrain and the forebrain of non-human primates and rats. Neurosci Biobehav Rev 20:593–605. [PubMed: 8994198]

Highlights

- Post-signal behavioral adjustment is central to cognitive control.
- Studies have described the neural bases of post-error slowing in the SST.
- Post-success slowing engaged a distinct network of left-hemispheric brain regions.
- The findings may have implications for computational modeling of SST performance.

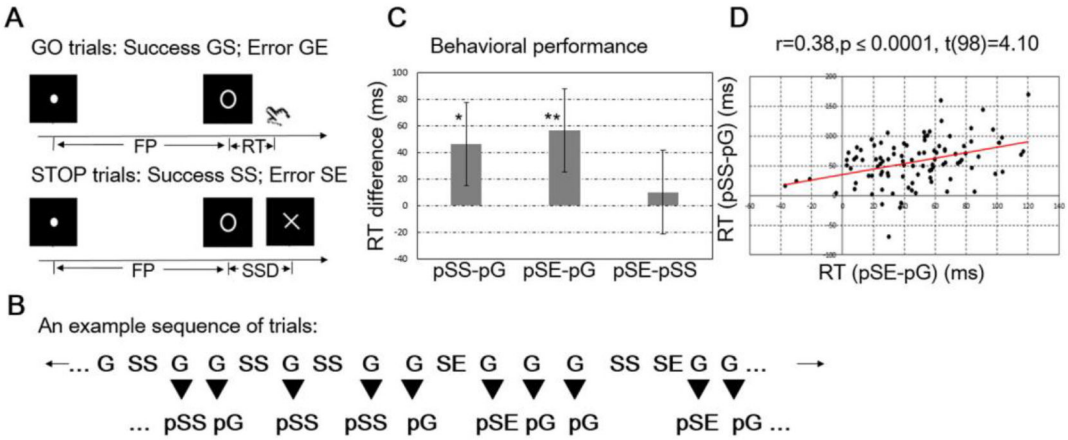

Figure 1.

The stop signal task (SST) and performance. (A) Behavioral paradigm; (B) A trial sequence to illustrate post-go (pG), post-stop success (pSS), and post-stop error (pSE) go trials; (C) Bar plots to show the extent of post-success slowing (PSS) and post-error slowing (PES) in mean ± S.D. across subjects: *p≤0.001 and **p≤0.0001; (D) A scatter plot to show the positive correlation between PSS and PES across subjects. Each dot represents data of one subject.

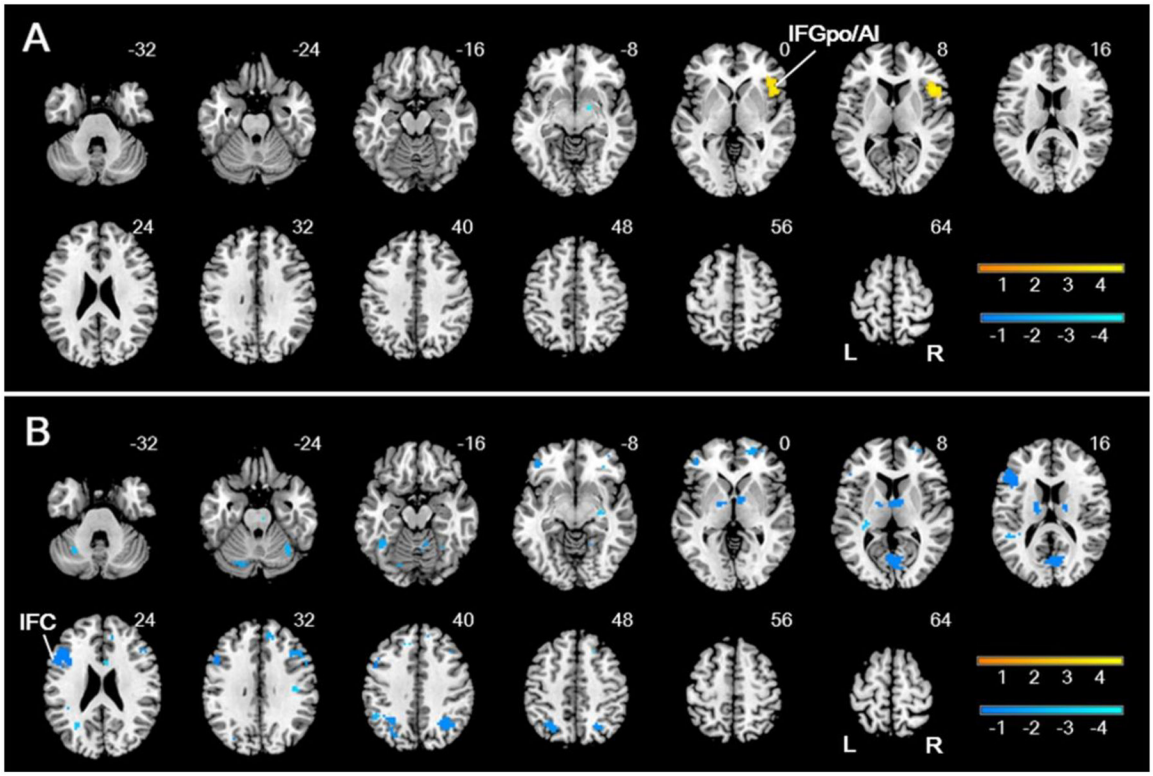

Figure 2.

Regional activations to post-error slowing (PES) and post-success slowing (PSS). IFGpo/AI: inferior frontal gyrus, pars opercularis/anterior insula; IFC: inferior frontal cortex. The results of contrast (A) pSEi vs. pSEni and (B) pSSi vs. pSSni, at $p \leq 0.001$, uncorrected, shown in axial sections from z=−32 to +64 and neurological orientation: R = right. Color scale reflects voxel T values.

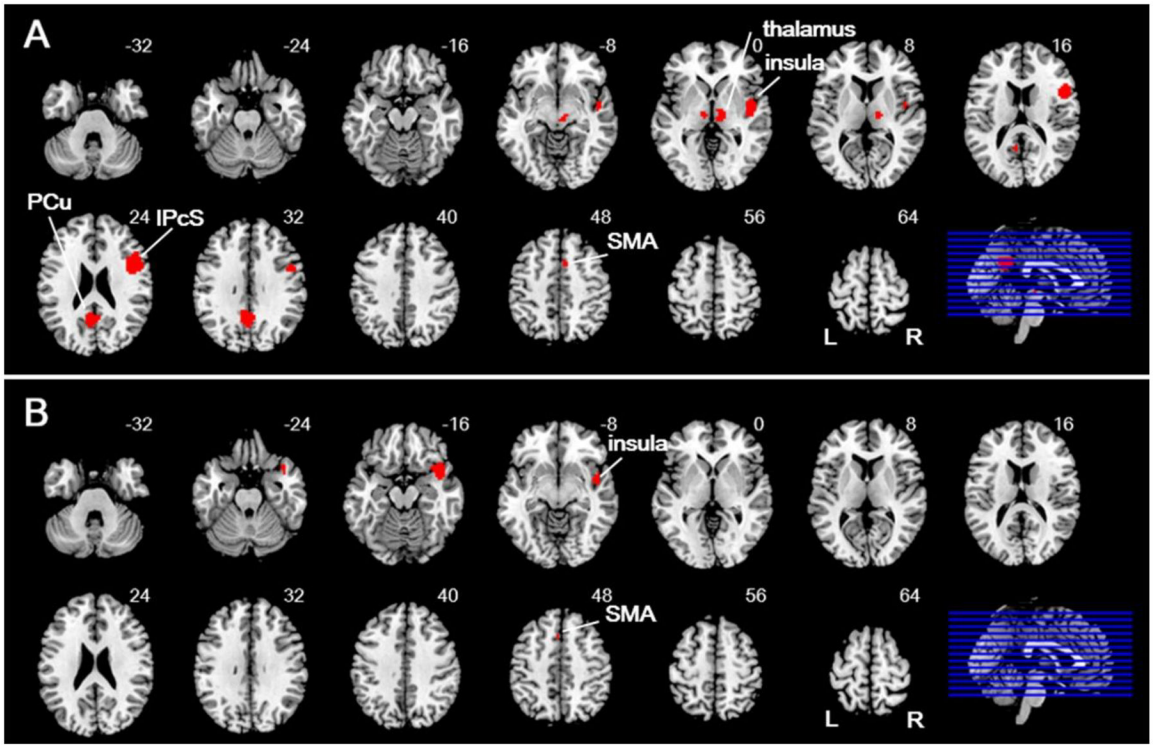

Figure 3.

Brain regions providing Granger causality inputs to (A) right IFGpo/AI, including the thalamus, right insula, right inferior precentral sulcus (IPcS), precuneus (PCu), and right supplementary motor area (SMA); and to (B) left IFC, including the right posterior insula and left SMA.

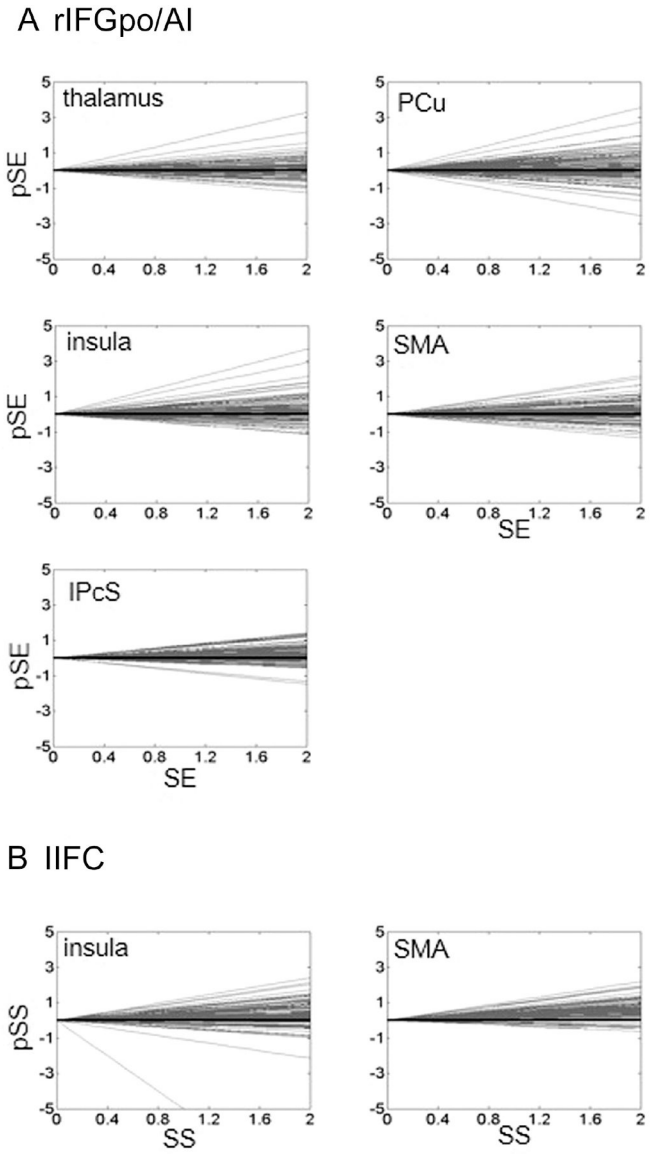

Figure 4.

Linear correlation of single trial amplitude (STA) between target region – right inferior frontal gyrus, pars opercularis and anterior insula (rIFGpo/AI) – and five input regions – thalamus, right insula, right inferior precentral sulcus (IPcS), precuneus (PCu), and the right supplementary motor area (SMA); as well as between target region – left inferior frontal cortex (lIFC) – and two input regions – insula and the left SMA. The regression lines are aligned at an intercept of zero for visualization of the overall pattern of slopes.

Table 1.

General Performance in the Stop Signal Task

GS (%)	SS (%)	Mean GoRT (ms)	Median GoRT (ms)	SERT(ms)	SSRT (ms)
93.7 ± 6.7	52.3 ± 2.7	616.1 ± 95.5	612.0 ± 103.4	552.0 ± 105.7	203.0 ± 34.7

Note: GS (%) and SS (%) = percentage of successful go and stop trials; GoRT = go trial reaction time; SERT = stop error reaction time; SSRT = stop signal reaction time

Table 2.

Regional activations to post-error slowing (pSEi > pSEni) and "deactivations" to post-success slowing (pSSni > pSSi) at voxel p≤0.001, uncorrected and cluster p≤0.05, FWE corrected.

Cluster Name	Cluster size (# voxels)	Cluster P value	Peak z value	MNI coordinate (mm)		
				X	Y	Z
		pSEi > pSEni, p≤0.001				
*right IFGpo/AI	114	0.002	4.66	45	17	7
			3.91	42	26	1
		pSSni > pSSi, p≤0.001				
*L IFC	229	0.0001	5.46	−45	26	19
			4.11	−51	14	22
			3.27	−48	11	40
Calcarine S	145	0.001	4.21	3	−70	10
R MFG	48	0.032	4.10	39	23	34
			3.55	48	23	31
			3.47	57	14	28
L OFG	48	0.032	4.05	−42	41	−2
			3.42	−35	47	−5
Thalamus	110	0.002	3.94	9	−1	1
			3.57	−18	−7	1
			3.55	−15	−7	13
Angular G	108	0.003	3.84	30	−64	46
			3.75	33	−58	40

Note:

*voxel p≤0.05, FWE corrected. All voxels with peaks 8 mm apart are identified. IFGpo/AI: inferior frontal gyrus, pars opercularis/anterior insula; L: left; IFC: inferior frontal cortex; R: right; S: sulcus; MFG: middle frontal gyrus; OFG: orbitofrontal gyrus; G: gyrus.